

# Preliminary Design Study of Asymmetric Hypersonic Inflatable Aerodynamic Decelerators for Mars Entry



*Space Systems Design Lab  
Georgia Tech Aerospace Eng.*

AE8900 MS Special Problems Report  
Space Systems Design Lab (SSDL)  
Guggenheim School of Aerospace Engineering  
Georgia Institute of Technology  
Atlanta, GA

Author:  
Brooke P. Harper

Advisor:  
Dr. Robert D. Braun

April 28, 2014

# Preliminary Design Study of Asymmetric Hypersonic Inflatable Aerodynamic Decelerators for Mars Entry

Brooke P. Harper<sup>1</sup> and Robert D. Braun<sup>2</sup>  
*Georgia Institute of Technology, Atlanta, GA, 30332*

The Mars missions envisioned in the future require payload mass in excess of the current capable limit for entry vehicle technology. Deployable Hypersonic Inflatable Aerodynamic Decelerators offer one solution to successfully improve drag performance and reduce ballistic coefficient to mitigate entry, descent, and landing concerns as payload mass increases. The majority of the research that has been conducted on these structures thus far only focuses on axisymmetric geometries. In this investigation, aerodynamic and aerothermodynamic performance is examined for three proposed asymmetric families that can generate non-zero lift-to-drag ratios at 0° angle of attack and are compared to a symmetric counterpart. Ideal results include favorable lift-to-drag ratios with reduced ballistic coefficients. The blunt, asymmetric Hypersonic Inflatable Aerodynamic Decelerator designs considered are assembled from stacked tori configurations with a base diameter of 20 m and the capability to interface with a 10 m diameter rigid center body. The configurations reviewed are capable of producing hypersonic lift-to-drag ratios between ~0.1 and ~0.6 for angles of attack ranging from -30° to 20°. A 40 Mt entry mass, approximate mass of large robotic or human scale mission is assumed. Advantageous ballistic coefficient data is retrieved for some asymmetric geometries. All HIAD configurations are determined to be statically stable as well. An initial assessment of the aerothermodynamic response predicts significant heating with radiative heating being much greater than convective heating. From the analyses completed thus far, encouraging results project asymmetric Hypersonic Inflatable Aerodynamic Decelerators as conceivable candidates for future large scale Mars missions.

## Nomenclature

$A$	=	reference area
$\alpha$	=	angle of attack
$\beta$	=	ballistic coefficient
$C_D$	=	drag coefficient
$C_L$	=	lift coefficient
$CG$	=	center of gravity
$C_m$	=	pitching moment coefficient
$C_{m,\alpha}$	=	pitching moment derivative with respect to angle of attack
$C_p$	=	pressure coefficient
$\gamma$	=	flight path angle
$h$	=	altitude
$L/D$	=	lift-to-drag
$M$	=	Mach number
$\rho_\infty$	=	freestream density
$q_\infty$	=	freestream dynamic pressure
$T_\infty$	=	freestream temperature
$V$	=	velocity

---

<sup>1</sup>Graduate Research Assistant, Guggenheim School of Aerospace Engineering, AIAA Student Member

<sup>2</sup>David and Andrew Lewis Associate Professor of Space Technology, Guggenheim School of Aerospace Engineering AIAA Fellow

## I. Introduction

ON August 6<sup>th</sup>, 2012 the world watched as one of the most daunting entry, descent, and landing (EDL) tasks in history was successfully executed with the Mars Science Laboratory (MSL). At 900 kg of payload mass, MSL likely represents the ceiling for landed mass with Viking-heritage EDL technology that has been a mainstay of Mars landers for decades.<sup>1,2</sup> As scientific curiosity about the red planet persists, the missions envisioned for future Mars robotic and human exploration will require significantly larger payload masses. Therefore, innovative ideas will need to be explored in order to accomplish prospective endeavors.

Specifically for Mars entry, the atmosphere is too thin (about 1% of Earth's) to provide substantial deceleration, yet it can generate considerable aerodynamic heating. In this environment, a sufficiently large drag area is necessary in order to reduce ballistic coefficient that relates inertial and drag forces. If this can be achieved in the hypersonic regime, ample deceleration on an entry vehicle can occur at high altitudes, and thus lengthen EDL timeline for subsequent maneuvering, lessen aerodynamic loading, and encounter a more benign thermal environment. For these beneficial attributes, future large robotic and human missions at Mars and other planetary bodies is practical.<sup>1</sup> For traditional rigid aeroshell systems, the maximum aeroshell diameter is limited by the launch vehicle payload fairing. MSL, for example, was limited to 4.5 m.<sup>2</sup> To bypass the payload fairing restriction, larger mass vehicles could use rigid, semi-rigid, or inflatable aerodynamic decelerators (IADs) to reduce their ballistic coefficient.<sup>3-9</sup>

Proposed for manned Earth re-entry and originally flown in the 1960's, IADs provide a low-volume, low-mass alternative to rigid bodies that assist with the deceleration of an entry vehicle prior to, or within an atmosphere by deploying inflatable structures with larger drag area than the entry vehicle's aeroshell alone. For this reason, the effort to resurrect IAD research has been strong over the past two decades.<sup>9</sup> According to the Entry, Descent, and Landing Systems Analysis Study (EDL-SA), some type of IAD implementation is an anticipated necessary component for high mass missions to Mars' surface.<sup>4,5</sup> In particular, Hypersonic Inflatable Aerodynamic Decelerators (HIADs) are one of the principal technologies currently analyzed to achieve mission enabling EDL architectures.

Flight tests conducted by the Aerodynamic Deployable Decelerator Performance-Evaluation Program (ADDPEP) as far back as 1966 provided pioneering research for HIADs. Coined "ballutes" at the time, ADDPEP investigated a five foot diameter ram-air inflated trailing isotensoid decelerator that experienced aerodynamic and aerothermodynamic loading at hypersonic speeds (up to Mach 9.7).<sup>10</sup> Though the article was not recovered, these initial tests provided a foundation for new HIAD designs and experiments to commence in the modern era.

Concepts such as the Inflatable Re-Entry and Descent Technology (IRDT), Mars Inflatable Aeroshell System (MIAS), and Inflatable Re-entry Vehicle Experiments (IRVE), shown in Fig. 1 have been established to further our knowledge and understanding of HIADs to mature development efforts.

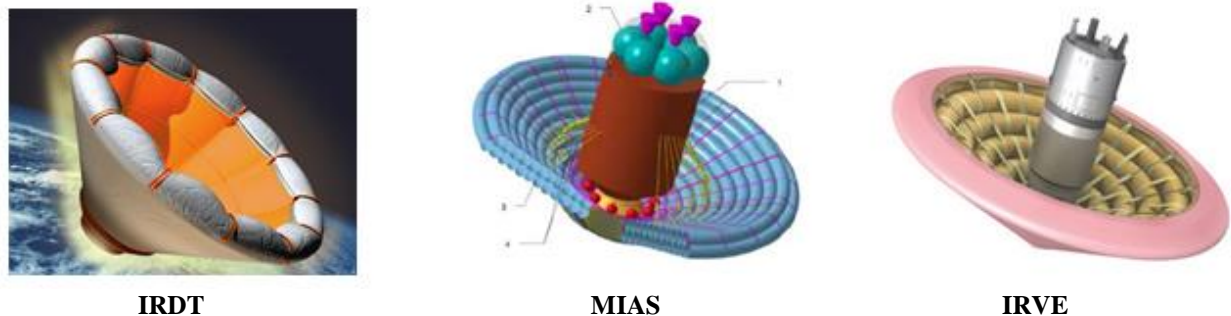


Figure 1. Present day HIAD concepts.

After a long drought in HIAD flight tests, the two-stage inflatable IRDT-1 system became the first mission to try and validate the feasibility of an attached HIAD during Earth re-entry in 2000. Unfortunately, unrelated to the inflatable itself, all attempts to recover viable data were failures.<sup>11</sup> Most recently, the IRVE program has taken the lead in HIAD research. Based off the MIAS design, IRVE is a 3 m diameter, 60° sphere-cone aeroshell formed by inflated stacked concentric tori. Through three missions, IRVE has effectively demonstrated various aspects of HIAD technologies including exo-atmospheric inflation, survivability of re-entry heating (at Earth) with flexible thermal protection systems (FTPS), aerodynamic stability, and the effect of lift, generated by a center of gravity offset. Plans for a fourth IRVE mission and the High Energy Atmospheric Re-entry Test (HEART), a larger

aeroshell with an entry mass on the order of 3.3 Mt are next in line to provide even more valuable information regarding HIADs.<sup>12</sup> With the accomplishments thus far, researchers have seen firsthand the benefits of HIADs and promote their applicability. They are now one possibility to integrate into future missions to Mars.

## II. Motivation and Significance

Current estimates for these large robotic or human-scale missions to Mars call for the landing of 40 - 80 Mt.<sup>1</sup> This study assumes that HIAD technology will provide the means for reducing the entry vehicle's ballistic coefficient in the hypersonic regime. As stated, a lower ballistic coefficient enables deceleration to occur higher in the atmosphere, providing additional timeline and altitude margin necessary for heavier payloads, as well as lower peak heat rate and integrated heat load. Furthermore, the EDL-SA study has established that the HIAD will be required to generate lift likely due to the following features a lifting body possesses:

- Additional EDL timeline
- Reduced gravity loads
- Lower peak heat rate
- Larger entry corridor
- Greater cross range and downrange capability
- Improved landed accuracy
- Mitigates uncertainty in navigation, atmosphere, and aerodynamics

To attain these characteristics, it is necessary to investigate potential outer mold lines (OML), or exterior shapes of an aeroshell, that predominantly determines the overall aerodynamic and aerothermodynamic performance of an entry vehicle. Because a HIAD acts as a temporary aeroshell that deploys exo-atmospherically from the entry vehicle body it is crucial to evaluate OML designs that will meet preliminary requirements for Mars entry.

In the 1950's, Allen Eggers made the discovery that changing the OML of a simple blunted cone to half of a rounded nose-cone shape that was flat on the top and round on the bottom could generate aerodynamic lift<sup>13</sup> and consequently a non-zero lift-to-drag ( $L/D$ ) at  $0^\circ$  angle of attack. Essentially, an asymmetric vehicle led to the inception of a lifting body. For all HIAD and Mars missions thus far, symmetric vehicles have flown, and therefore have had to impose a center of gravity offset to invoke an angle of attack and provide a lift force. To circumvent this manipulation, an asymmetric HIAD can be used to generate lift that is inherent to its geometry.

This study assesses the candidacy of three blunt, asymmetric HIAD families proposed for Mars entry by evaluating intrinsic aerodynamic and aerothermodynamic characteristics for each configuration and making comparisons to a symmetric counterpart. The reference area of these asymmetric designs will be equal to or less than that of the symmetric counterpart. Therefore, this investigation primarily focuses on improving drag coefficient ( $C_D$ ) by manipulation to HIAD shape alone. Other factors such as static stability and response to heating are also examined. The objective is to quantify advantages offered by these asymmetric HIAD with respect to a baseline symmetric HIAD.

## III. HIAD Outer Mold Line Geometry

### A. Symmetric HIAD – Baseline

The HIAD geometries proposed in this study are all derivatives of a symmetric, 20 m diameter, blunted  $50^\circ$  sphere-cone capable of interfacing with a 10 m diameter rigid center body. The HIAD height is constrained to 4 m for all configurations. A series of stacked inflatable concentric tori tied to each other and to the vehicle are used to define the structure of each of these HIADs. This assembly will maintain the desired shape of the aeroshell under aerodynamic load. A flexible thermal protection system blanket is presumed to tightly cover the HIAD body. A rigid nose cap attachment is assumed. The cross section of the symmetric HIAD is represented in Fig. 2.

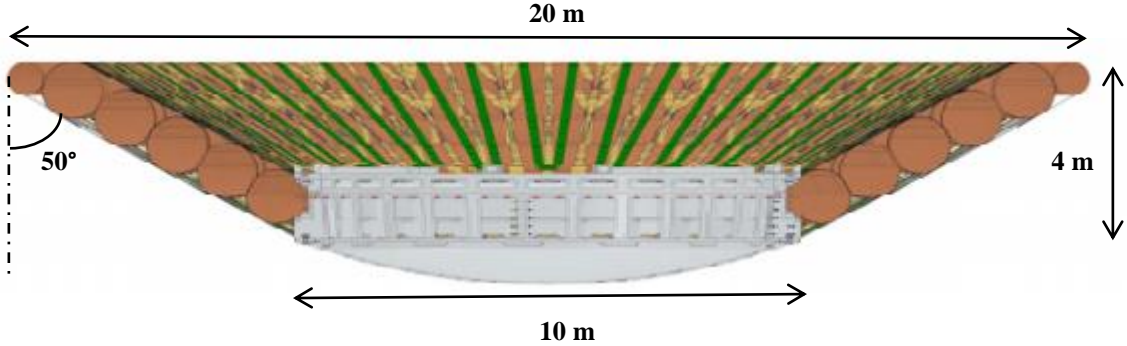


**Figure 2. Baseline symmetric HIAD cross section.**

For the following geometries, this baseline design is initially generated and then geometric manipulations occur to produce asymmetric configurations driven by potential advantages of increased  $L/D$ , ideally with larger  $C_D$ , smaller trim angles, and reduced heating.

### B. Shifted HIAD Family

Shifted HIADs are constructed by defining a shift as a percentage of one-fourth the base diameter (5 m). When a shift is implemented, the base torus translates through the initial longitudinal axis of symmetry by the amount of the shift specified and the intermediate tori follow to maintain geometry. For instance, if a 100% shift is applied, the tori are oriented in a way such that one edge is aligned horizontally. Figure 3 shows the Shifted HIADs that are analyzed in this study.

As a shift is defined, the nose radius must be controlled in order to maintain smooth connection between the HIAD frustum and nose cap. These adjustments are minor, only slightly changing the overall OML from one Shifted HIAD to another. This trivial variance in the rigid nose cap is deemed negligible.

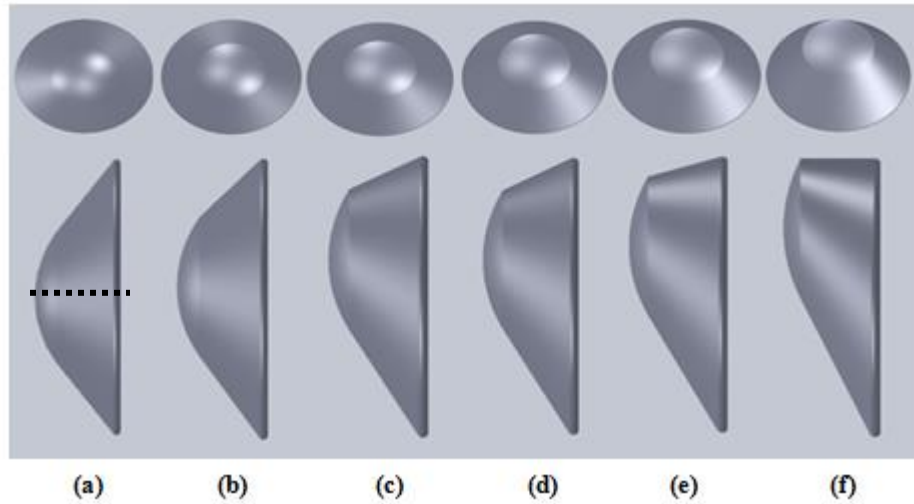


**Figure 3. Top and side views of Shifted HIADs at (a) symmetric, (b) 20%, (c) 40%, (d) 60%, (e) 80%, (f) 100%.**

### C. Flat HIAD Family

Much like Eggers' lifting body geometry, a second asymmetric HIAD OML is generated by terminating the tori at a specified length along the 20 m base diameter. All tori larger than the defined length are essentially cut to

produce a flat top. The result of this process is displayed in Fig. 4 with Small, Medium, and Large Flat HIADs. The lengths chosen to yield these designs were  $18\frac{1}{3}$  m,  $16\frac{2}{3}$  m, and 15 m respectively.

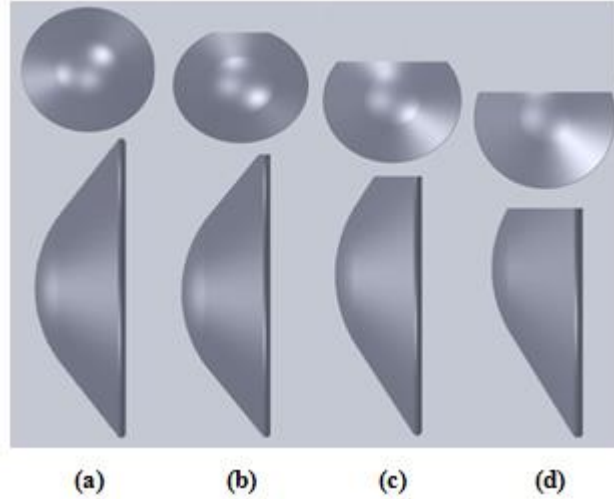


**Figure 4. Top and side views of Flat HIADs for (a) symmetric, (b) Small, (c) Medium, (d) Large.**

The Flat HIAD family was created to exploit the favorable thermal characteristics a flat plate possesses. However, by this method, the reference area is reduced in comparison to the symmetric HIAD. While the drag area is less with each cut, it is possible that the resulting  $L/D$  and  $\beta$  does not deviate considerably from the symmetric baseline. For the anticipated heating challenge at Mars, an aerothermodynamic benefit may greatly outweigh the slight aerodynamic variances. It is important to note that the manufacturability of these asymmetric components raises the complexity of such a design.

#### D. Biconic HIAD Family

Biconic HIADs are produced by slicing through the top of an original symmetric HIAD at specified angles. The cases examined in this study are  $30^\circ$ ,  $20^\circ$ , and  $10^\circ$  planar cuts along the top of the HIAD to produce biconic shapes seen in Fig. 5.

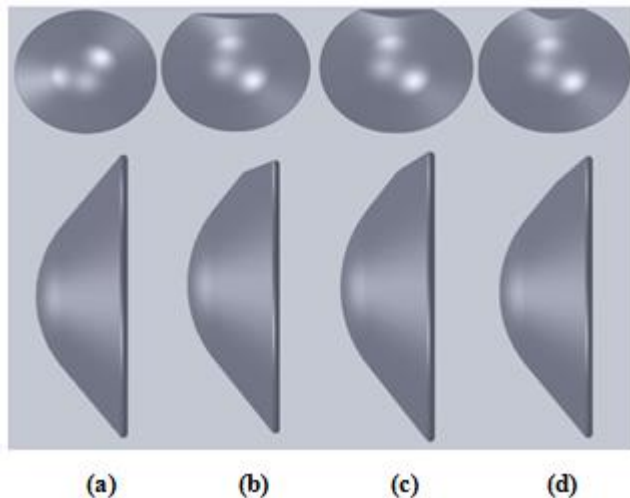


**Figure 5. Top and side views of Biconic HIADs at (a) symmetric, (b)  $30^\circ$ , (c)  $20^\circ$ , (d)  $10^\circ$ .**

These slices are made at the midpoint height of the HIAD frustum. The maximum allowable biconic configuration is a  $50^\circ$  (sphere-cone angle) planar cut which will then resemble a Flat HIAD OML. Like the assumptions made for the Flat HIAD configuration, the objective is to maintain respectable aerodynamic performance but gain improved aerothermal response.

## IV. Methodology

### A. Aerodynamics and Stability

The pressure distribution on the HIADs is approximated using a modified Newtonian<sup>14-16</sup> panel method that allows the forces and moments to be determined from shape alone. The pressure coefficient,  $C_p$ , is defined by the fluid flow normal to the HIAD surface. This is based on the assumption that the fluid momentum normal to the aeroshell is lost upon impacting the surface of the body, while the tangential component is conserved. A mesh of each HIAD design was generated to calculate the unit inward normal and  $C_p$  for each mesh panel. Aerodynamic forces are computed through numerical integration of  $C_p$  over the surface of the HIAD body. Performance measures of interest are deduced including  $L/D$ ,  $C_D$ , and the hypersonic ballistic coefficient  $\beta$  governed by

$$\beta = \frac{m}{c_D A} \quad (1)$$

where  $m$  is the entry mass and  $A$  is the reference area of the HIAD. The magnitude of deceleration and the heating profile associated with the hypersonic regime are strong functions of these parameters. Equation (1) shows that increasing the drag area will reduce the ballistic coefficient. As such, increasing the diameter of an entry system beyond that allowed by the vehicle fairing would reduce the ballistic coefficient (for a fixed shape).

The aerodynamic characteristics were determined over angle of attack  $\alpha = -30^\circ$ – $20^\circ$  and constant  $C_{p,\max} = 2$  to allow for Mach number independence consistent with modified Newtonian theory. The range of positive  $\alpha$  is included to show that the asymmetric shapes are capable of attaining positive  $L/D$ . Sideslip and bank angles are not modeled. A 40 Mt entry mass was assumed and the inflatable itself will add a negligible amount of mass to this type of payload. Therefore, the mass of the inflatable and its components is not studied.

Due to the asymmetric nature of the HIADs, there is concern about the stability of each configuration throughout flight in the hypersonic regime. The stability of any entry system is a vital factor in determining whether a particular design is feasible. Static stability is achieved when

$$C_{m_\alpha} = \frac{dC_m}{d\alpha} < 0 \quad (2)$$

where  $C_m$  is the pitching moment about the center of gravity (CG) as shown in Fig. 6. Therefore, we can say that static stability is solely a function of the CG. The parameter innate to a statically stable vehicle is the trim angle, or the angle at which a vehicle returns to after encountering flight disturbances. Determining the vehicle's trim angle is significant. It can effectively move the stagnation point and increase the possibility of transition to turbulence on the vehicle which promotes negative attributes, such as higher heating and wake flow impingement on the payload.

For each HIAD geometry, the angle of attack corresponding to  $L/D = 0.275$ , an average of proposed nominal  $L/D$  for large payloads at Mars,<sup>1,4,17-19</sup> is assigned as the trim angle. This assignment anchors the location of the center of pressure ( $CoP$ ), or the point at which the aerodynamic forces act through, and allows the CG to be determined by realizing where aerodynamic moments equal zero about an array of CG locales. The allowable CG locations represent where payloads can be effectively packaged. The acceptable CG locations over the body produce a fit CG trim line. Favorable trim lines, ones which

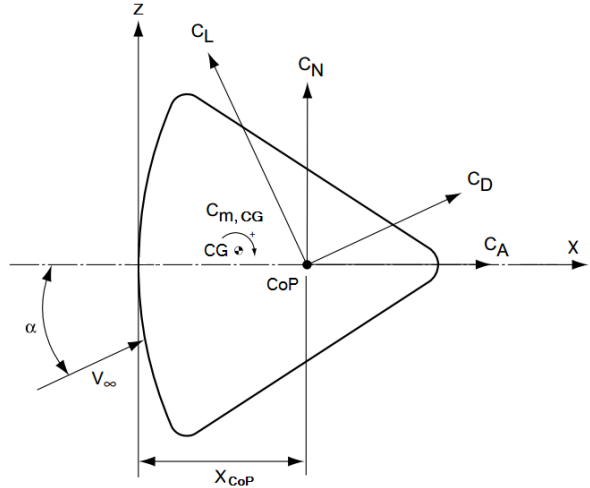


**Figure 6. Free body diagram of forces and moments acting on an entry vehicle at angle of attack.**

allow for flexible payload placement, are anticipated for most HIAD geometries analyzed. If adequate trim lines result, the payload within the entry vehicle may not require complex packaging. An ideal aeroshell shape would achieve this specified  $L/D$  while maximizing  $C_D A$  (thereby minimizing  $\beta$ ) and be statically stable at the trim attitude.

## B. Aerothermodynamics

The anticipated environment and flight conditions HIADs will be exposed to during Mars entry is intimidating from an aerothermodynamic perspective. Due to their large size, high entry velocities, and non-zero angle of attack a number of challenges are posed. Catalytic heating due to recombination of dissociated species will become a much more substantial factor than with smaller, previous missions to Mars' surface. Accordingly, thermochemical non-equilibrium effects within the shock-layer will result and its effects will need to be well understood. Additionally, due to high Reynolds numbers, it is expected that the vehicle will experience boundary-layer transition to turbulent flow well before the peak heating point on the trajectory.<sup>20,21</sup> Furthermore, radiative heating will be appreciable, potentially larger than the convective heating.<sup>22</sup> With such complex flow behavior, typical engineering correlations for heating such as Sutton-Graves and Tauber-Sutton equations which rely on thermochemical equilibrium stagnation point flow become inadequate for the complex flow conditions projected for HIADs. Therefore, computational fluid dynamics (CFD) tools must be enabled to seek out a more reliable response to such a flow.

CFD programs integrate high-fidelity numerical methods to simulate fluid flow at specified flight conditions. Calculations were performed first with CBAERO and then with Langley Aerothermodynamic Upwind Relaxation Algortihm (LAURA). The model assumptions<sup>23</sup> are as follows:

- Turbulent boundary layer: Baldwin-Lomax model implemented
- Chemical non-equilibrium using the Micheltree and Gnoffo<sup>24</sup> 8-species Mars model ( $\text{CO}_2$ ,  $\text{CO}$ ,  $\text{N}_2$ ,  $\text{O}_2$ ,  $\text{NO}$ ,  $\text{C}$ ,  $\text{N}$ ,  $\text{O}$  with 97% and 3% freestream mass fractions for  $\text{CO}_2$  and  $\text{N}_2$  respectively)
- Thermal non-equilibrium (two temperature)
- Radiative equilibrium wall, emissivity  $\epsilon = 0.89$
- Super-catalytic wall: recombination of  $\text{CO}_2$  and  $\text{N}_2$  to freestream mass fractions
- Non-blowing smooth wall

### 1. Defining Flight Conditions

To date, no mission has come close to the magnitude of the proposed high mass entry. The suggested HIADs are nearly five times as large as MSL in size, decelerating 40 times the payload mass, and will have entry velocities predicted upwards of 8500 m/s. For this reason, indentifying flight conditions where peak heating is experienced is very difficult. As a first-order approach, a 3-DOF trajectory simulation is employed with the symmetric HIAD to seek out an accurate window where peak heating may result for all configurations. The standard Mars Pathfinder atmosphere model is used with  $V_{\text{entry}} = 8500 \text{ m/s}$  and  $\gamma = -15.5^\circ$ . Table 1 shows an estimated range where peak heating should be captured. These flight conditions were used with CBAERO to build an aerothermal database to condense the range of flight conditions that provokes high heating.

**Table 1. Window of flight conditions where peak heating may result.**

Parameter	Peak Heating Window
$M$	30-55
$V$	6.3-8.1 km/s
$q_\infty$	1-25 kPa
$\rho_\infty$	$5 \times 10^{-5} - 2 \times 10^{-4} \text{ kg/m}^3$
$T_\infty$	120-170 K
$h$	30-80 km

## 2. CBAERO

The Configuration Based Aerodynamics (CBAERO)<sup>25,26</sup> software package is an engineering level tool that provides rapid analysis for aerodynamic and aerothermodynamic behavior for general vehicle configurations in atmospheric entry environments. CBAERO makes use of an unstructured surface grid of triangles to define the Outer Mold Line of the vehicle configuration. No volume mesh is required. Surface-based techniques, including modified Newtonian panel method, are applied to estimate surface pressure field and streamline patterns. Engineering correlations<sup>27,28</sup> are then applied along these surface streamlines to provide wall temperature, convective, and radiative heating estimates and other surface properties.

## 3. LAURA

Langley Aerothermodynamic Upwind Relaxation Algorithm (LAURA)<sup>29-31</sup> is a high fidelity, structured, multi-block Navier-Stokes aerothermodynamic simulation tool. It is specialized for multi-physics coupling, utilizing advanced numerical methods for computational fluid dynamic (CFD) simulations. It has been extensively used to predict the aerodynamics and aerothermodynamics for Mars entry vehicles.<sup>32-34</sup> The code uses a finite-volume shock-capturing approach to approximate hypersonic flow effects with frozen, equilibrium, or non-equilibrium thermochemistry. Fundamental elements of LAURA include Roe's averaging<sup>35</sup> and Yee's Symmetric Total Variation Diminishing (STVD)<sup>36</sup> formulation of second-order, inviscid flux.

## 4. Structured Grid Generation

GridGen<sup>37</sup> was used to develop multi-block, structured grid topologies for one geometry in each HIAD family. Special care needs to be taken to define grid lines that are nearly orthogonal to the body surface. It should also be recognized that grid adaptation can produce negative volumes if there is poor topology. Therefore, structured grid generation is still one of the more timely aspects of CFD. For hypersonic flow, only the forebody is modeled with a farfield that extends far enough out so shock cannot quickly escape the domain. Symmetry about the y-axis can be enabled to reduce the number nodes. Grids are on the order of 150,000-170,000 nodes and are made viscous by distributing 96 normal nodes with very small spacing near the surface. Figure 7 shows each of the generated grids.

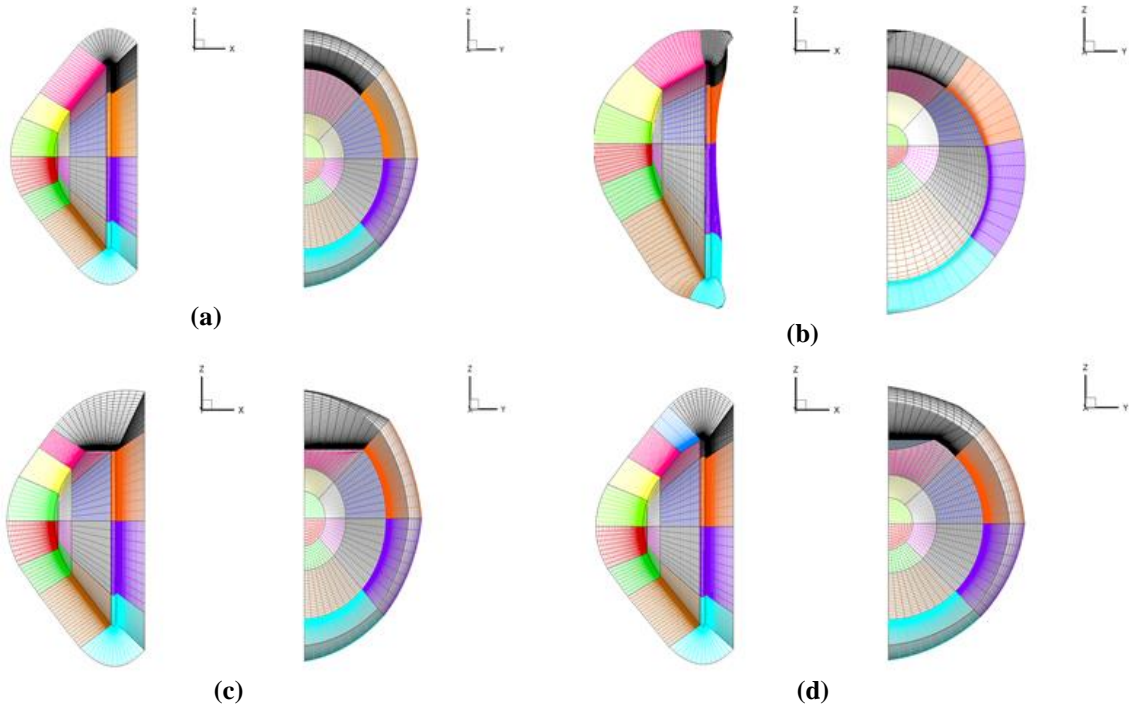


**Figure 7.** Grid topologies for (a) Symmetric, (b) 60% Shifted, (c) Medium Cut Flat, and (d) 20° Biconic HIAD.

## V. Results

### A. Hypersonic Aerodynamic Force Coefficients

#### 1. Shifted HIADs

In comparison to the symmetric HIAD, Fig. 8a and b clearly show that as shift is applied  $C_L$  increases over all angles of attack and  $C_D$  has the capability to exceed the baseline values. This is due to the fact that the symmetric HIAD produces a large negative normal force that dictates both its lift and drag capability. At  $\alpha = -30^\circ \sim -15^\circ$  Shifted HIADs produce higher  $C_L$  coefficients from the combination of having smaller negative, or even positive normal forces and almost invariant axial forces with respect to the symmetric case. Once out of that range, the Shifted HIADs begin to produce axial forces that dominate the symmetric HIAD lift component that previously allowed greater  $C_D$  to be obtained over larger angles of attack. By  $\alpha = -10^\circ$  all Shifted HIAD cases analyzed surpass the symmetric HIAD  $C_D$ . This trend allows improved  $L/D$  performance to be captured at smaller angles of attack as seen in Fig. 8c. It should also be noted that small magnitudes of positive  $L/D$  can be achieved at positive angles of attack for some Shifted HIAD cases.

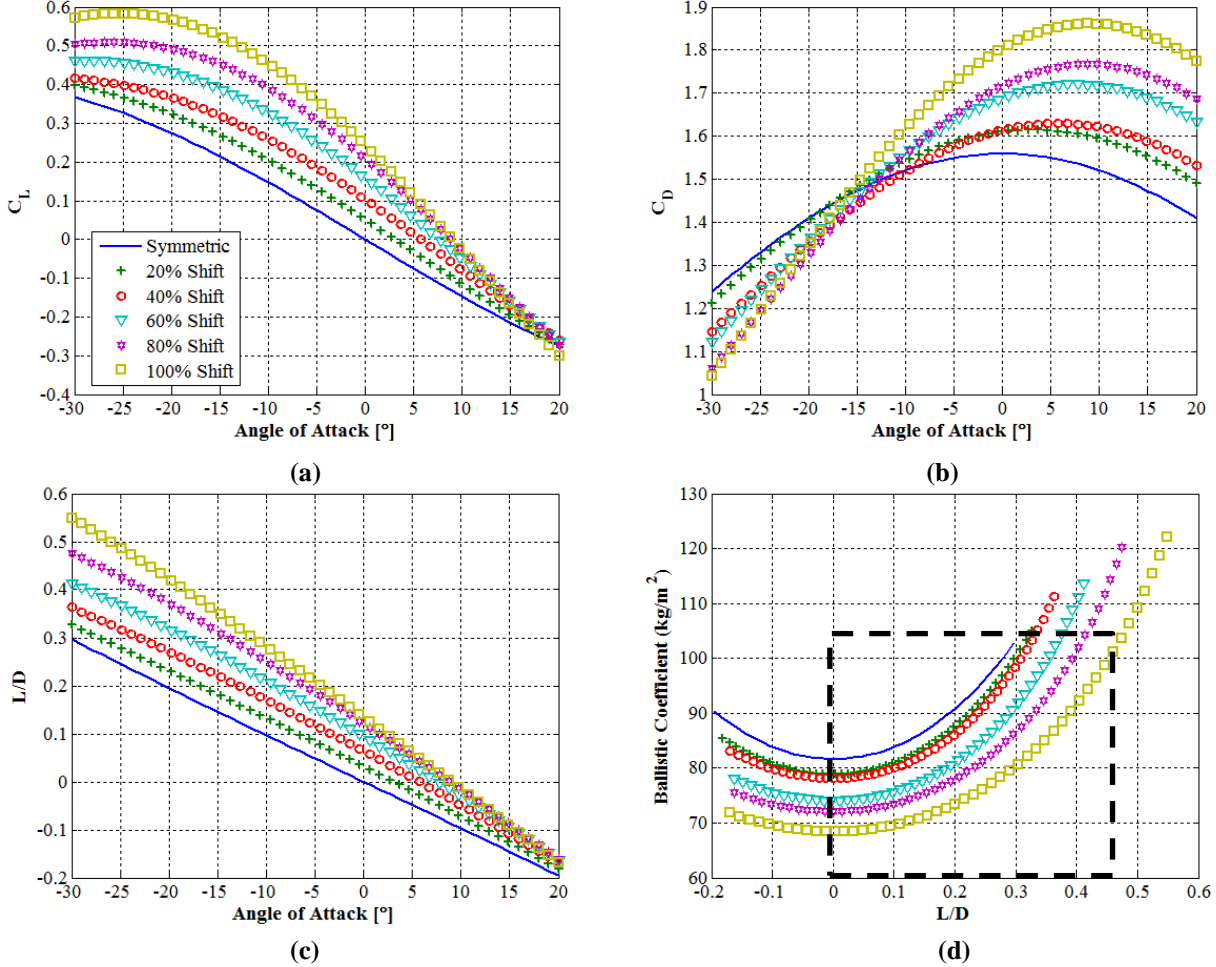


**Figure 8. Aerodynamic data for Shifted HIADs (a)  $C_L$ , (b)  $C_D$ , (c)  $L/D$  vs. angle of attack, and (d)  $\beta$  vs.  $L/D$ .**

This information alone is not enough to understand the advantages of this trend. To accurately depict the benefits of using a Shifted HIAD the tradeoff between  $L/D$  and  $\beta$  is examined in Fig. 8d. The results captured in the boxed region from  $L/D = 0 \sim 0.46$  exhibit where every Shifted HIAD case promotes ideal aerodynamic features (i.e. improved  $L/D$  performance at reduced  $\beta$ ). As shift increases, the benefits become steadily more apparent. The area

outside the box highlights where higher angles of attack enhanced  $L/D$  at the expense of  $C_D$  and ultimately higher  $\beta$ , or negative  $L/D$  occurs.

For  $L/D = 0.275$  (that proposed for high mass Mars entries), Shifted HIADs meet the goal of increasing  $L/D$  performance by amplifying both  $C_L$  and  $C_D$  while decreasing  $\beta$ . Furthermore, because this occurs at lower angles of attack, the trim angles necessary for stability will be lessened. A stability analysis investigating the effects of these trim angles follows. From an aerodynamic standpoint, Shifted HIADs are potentially promising candidates for Mars entry.

## 2. Flat HIADs

As anticipated, aerodynamic results for Flat HIADs are dominated by their reduction in reference area. To offset the loss in area,  $C_D$  would have to greatly outweigh the symmetric counterpart in order to see  $\beta$  decrease. While the force coefficients in Fig. 9a-c resemble the trend of the Shifted HIADs, the first instance where  $C_D$  exceeds the symmetric case is not until  $\alpha \approx -6^\circ$ . Therefore, there is only a very small region where  $L/D$  is improved by way of both an increase in both  $C_L$  and  $C_D$ .

It is important to examine the effects of this loss in area in Fig. 9d. The rise in  $\beta$  is not drastic. Even for the Large Flat HIAD where  $C_D$  is significantly smaller than that of the symmetric HIAD, variation in  $\beta$  is not large. However, it would likely become a concern if  $L/D > 0.3$  is a requirement.

These configurations are not aerodynamically superior to symmetric HIADs but may be able to compensate for these losses by showing favorable stability for sufficient packaging and the ability to withstand the harsh aerothermal loads expected in any entry mission.

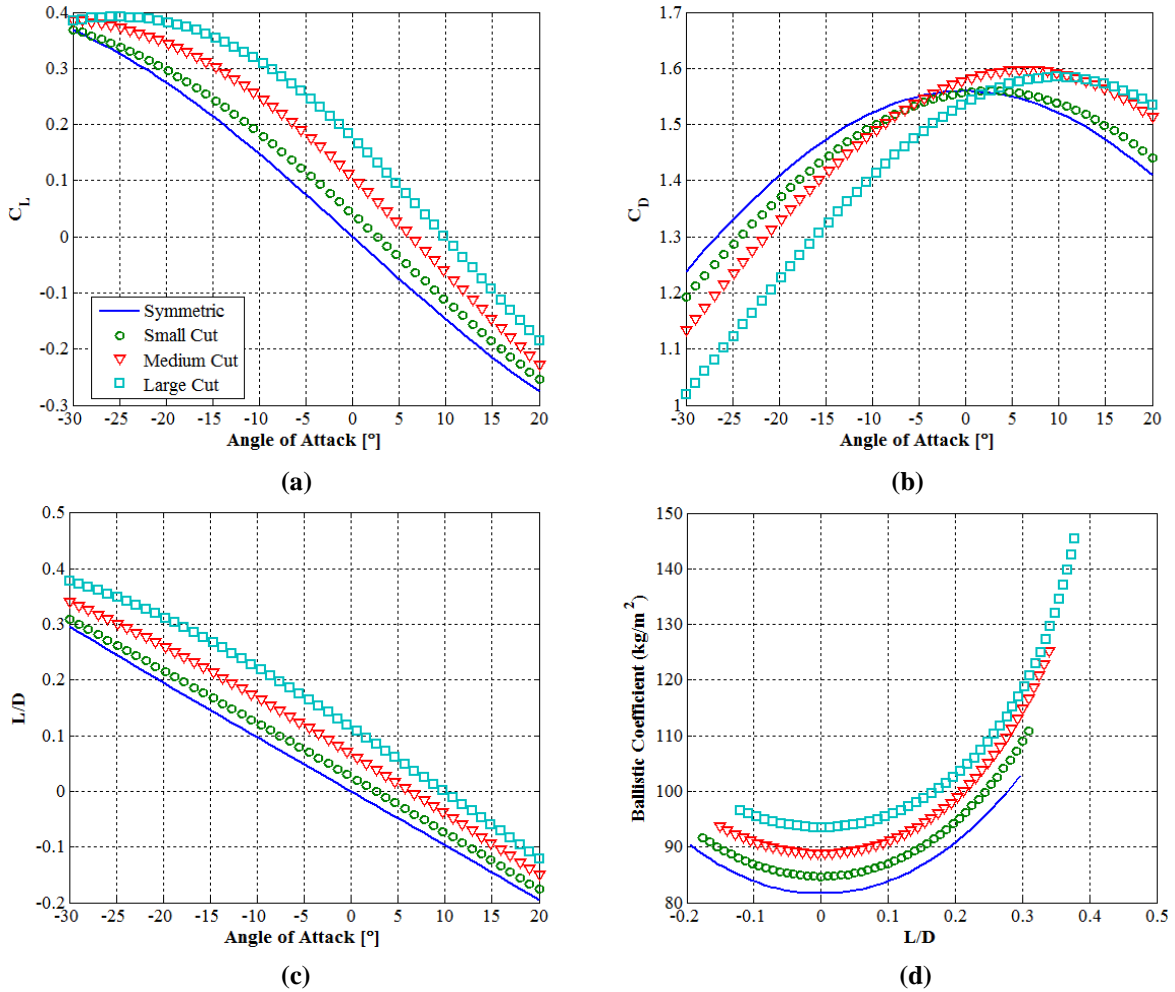


**Figure 9. Aerodynamic data for Flat HIADs (a)  $C_L$ , (b)  $C_D$ , (c)  $L/D$  vs. angle of attack, and (d)  $\beta$  vs.  $L/D$ .**

### 3. Biconic HIADs

The aerodynamic response for Biconic HIADs is analogous to the Flat HIADs. The slight loss in reference area does not strengthen any aerodynamic properties of interest. In fact, as shown in Fig. 10a-d, there is not much gained at all from this type of design manipulation. The  $L/D$  captured is nearly identical to the symmetric HIAD and  $\beta$  is increased for each case. This is not to say the Biconic HIADs are an overall weak choice, they just do not exemplify overall better aerodynamic performance.

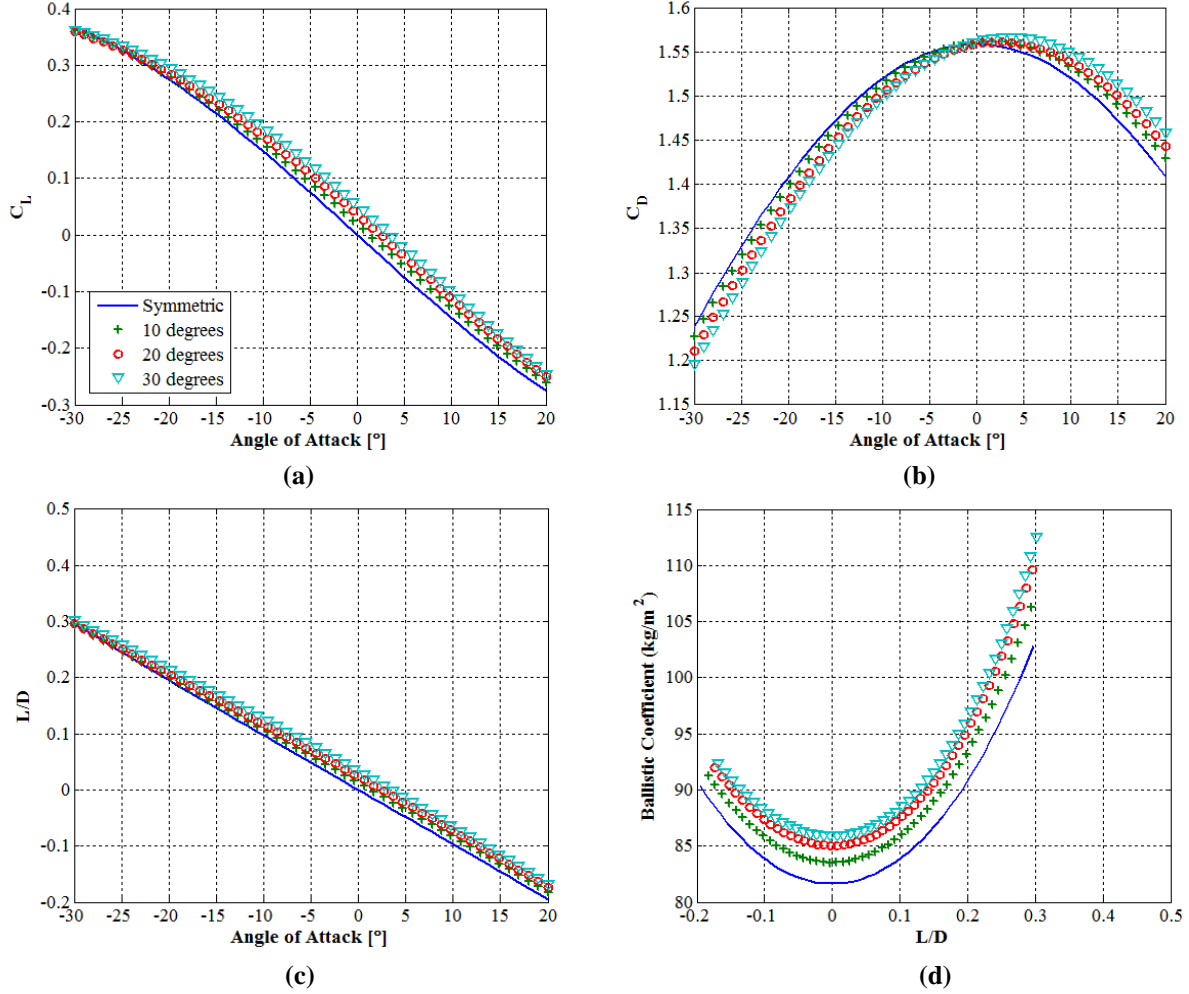


**Figure 10.** Aerodynamic data for Biconic HIADs (a)  $C_L$ , (b)  $C_D$ , (c)  $L/D$  vs. angle of attack, and (d)  $\beta$  vs.  $L/D$ .

### 4. Force Coefficient Summary

In general, for all asymmetric HIAD cases analyzed,  $L/D$  performance is enhanced. However, for the majority of configurations investigated it is attributed to large  $C_L$  and low  $C_D$  values, which is not ideal. There was encouraging data retrieved from the Shifted HIAD family where  $L/D$  was improved with coupled reduction in  $\beta$ . When  $L/D = 0.275$  is required, many asymmetric HIADs are capable of producing greater drag. However, for the Flat HIAD cases that have this characteristic, their reduction in area does not allow  $\beta$  to decrease. Table 2 shows the differences with these two attributes at that flight constraint.

**Table 2. Percent increase/decrease with respect to the symmetric HIAD  $C_D$  and  $\beta$  at  $L/D = 0.275$**

Configuration	Drag Coefficient (%)	Ballistic Coefficient (%)
Symmetric	<b>1.2785</b>	<b>99.59 (kg/m<sup>2</sup>)</b>
20% Shift	+ 3.25	- 3.15
40% Shift	+ 5.09	- 4.85
60% Shift	+ 13.03	- 11.54
80% Shift	+ 18.62	- 15.69
100% Shift	+ 27.22	- 21.40
Flat Small Cut	- 1.20	+ 4.99
Flat Medium Cut	+ 1.22	+ 9.91
Flat Large Cut	+ 2.43	+ 13.60
Biconic 10°	- 0.95	+ 3.49
Biconic 20°	- 1.87	+ 6.30
Biconic 30°	- 1.84	+ 7.71

## B. Hypersonic Static Stability

A stability analysis was also conducted under the assumption that the entry architecture targets a nominal  $L/D = 0.275$ . For each HIAD design, the angle of attack that coincides with that  $L/D$  was interpolated and assigned as the trim angle. Table 3 shows each respective trim angle for all configurations.

**Table 3. Trim angles at  $L/D = 0.275$  for each HIAD geometry**

Configuration	Trim Angle (at $L/D = 0.275$ )
Symmetric	<b>-27.9</b>
20% Shift	-24.6
40% Shift	-20.4
60% Shift	-16
80% Shift	-12
100% Shift	-9.6
Flat Small Cut	-26.24
Flat Medium Cut	-21.75
Flat Large Cut	-15.51
Biconic 10°	-27.9
Biconic 20°	-27.6
Biconic 30°	-26.8

With the exception of the Biconic 20° case, all asymmetric HIADs achieve a smaller trim angle than the symmetric counterpart. This is a beneficial attribute that will likely lead to reduced aerothermal and lateral aerodynamic loading on the leeside of the HIAD. The stability corresponding to these trim angles are however unknown. Thus, an exploration to determine potential CG locations corresponding to these trim angles is necessary in order to establish locales where  $C_m = 0$  and confirm stability requirements. Moreover, the location of the CG is examined as it is a significant factor in deciding how the payload can be effectively packaged.

The lift and drag forces that act through the center of pressure produce the moments that act on the CG. An iterative approach was implemented to seek out the coordinates of several CG locations along the HIAD body. Linear fit CG trim lines result and are depicted in Fig. 11. The dotted black lines represent the boundaries of 10 m rigid body.

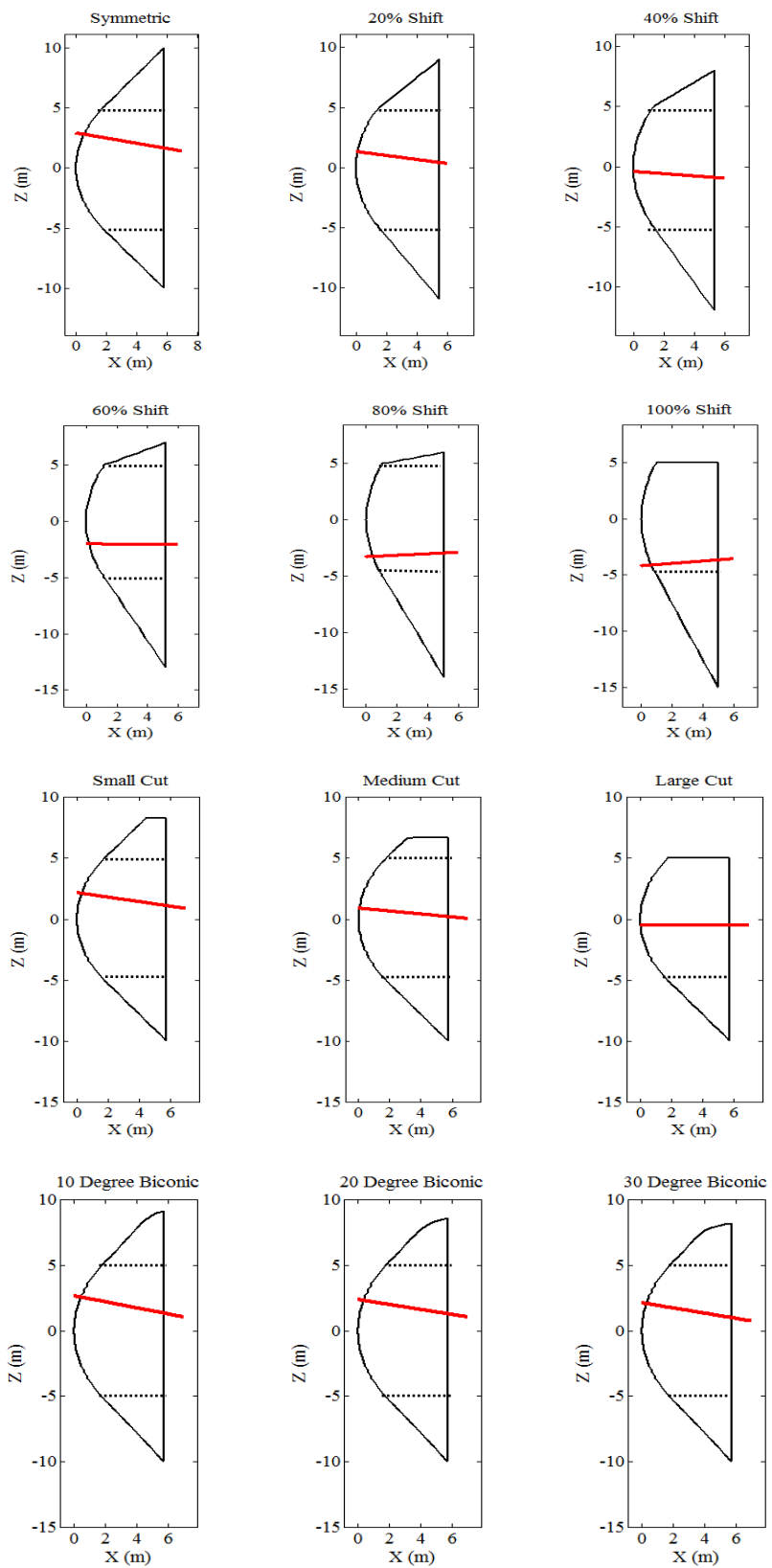


**Figure 11. Center of gravity trim lines capable of trim angles of attack where  $L/D = 0.275$ .**

For all HIAD families, CG trim lines exist through the 10 m rigid center body. The Shifted HIADs exhibit the most interesting trend. As shift increases, the slope of the CG trim line becomes less negative until it reaches approximately zero at 60% and thereafter at 80-100%, has a positive slope near the rigid body interface. This outcome is the least suitable of all OML geometries. Efficient packaging is more difficult to attain if the allowable CG locations reside where there is only a narrow amount of space available for payload. Flat HIADs behave in a similar manner, providing more flexibility than both the symmetric and Shifted HIADs. The Large Cut yields the most advantageous array of CG locations for payload placement as the CG trim line nearly extends horizontally from the nose of the vehicle. Assuming a symmetric payload, the CG can be placed along this axis. Lastly, as expected, the Biconic HIADs do not deviate much from the symmetric case. It should be noted that once the HIAD is jettisoned, new aerodynamic forces and moments will be produced which would change the stability of the entry vehicle along its trajectory.

To ensure that these are statically stable vehicles,  $C_m$  curves were generated over a range of angle of attack. A random CG coordinate from each CG trim line was coupled into the modified Newtonian model. Figure 12 shows where each configuration experiences  $C_m = 0$  and matches the values in Table 3. Likewise, it is evident that  $\frac{dC_m}{d\alpha} < 0$ . It should be recognized that there is slight discrepancy between the trim angles stated for the 80% and 100% Shifted HIADs. This is believed to originate from the iterative procedure not being able to minimize moments at precisely zero for these configurations.

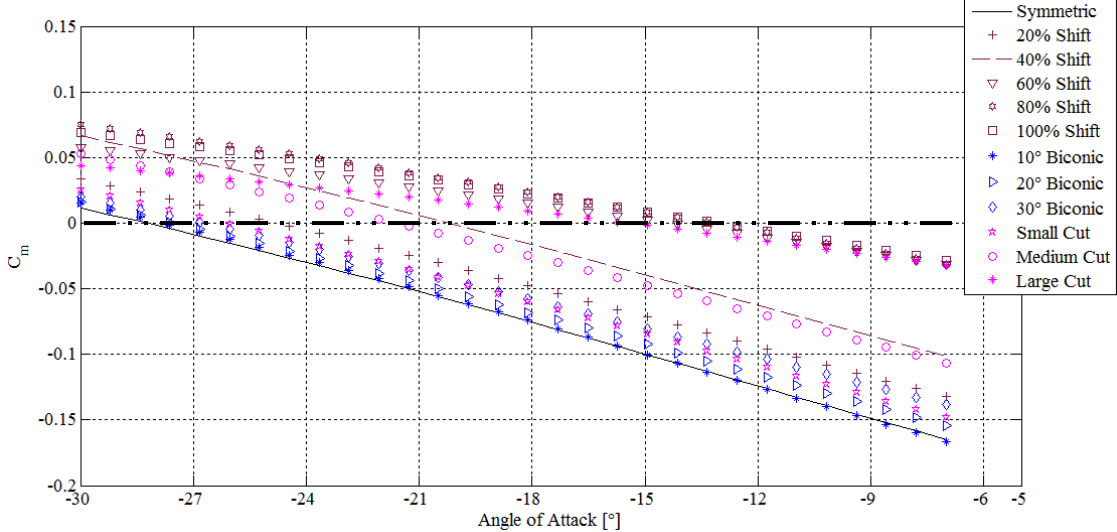


**Figure 12.**  $C_m$  curves for each configuration over a range of angle of attack.

### C. Heating Estimates and Ramifications

The aerothermal database produced by CBAERO allowed the flight condition ranges where peak heating may occur to shrink. All cases with  $M > 40$  were thrown out. The software implies that the peak heating values occur at  $M=39$  and  $q_\infty = 21 \text{ kPa}$ . Figure 13 shows convective and radiative heating for the symmetric case.



**Figure 13.** Radiative and convective heating for the symmetric HIAD.

This result shows that the radiative heating is significant as it is roughly 1.5 times the magnitude of the convective heating. The leeside of the vehicle is where this peak heating is incurred. This makes sense due to the angle of attack the HIAD is entering at. The asymmetric HIADs follow this trend as well. However, the heating results for these geometries are questionable and might be invalid. The approximations made by the rapid algorithms imply that the Flat and Biconic HIADs have considerably greater radiative and convective heating. While a slight increase may be true due to their higher  $\beta$ , the heat transfer off the biconic and flat surfaces is not accounted for correctly. As for the Shifted HIAD, radiative heating has been marginally lowered, but convective heating is raised. The LAURA simulations should provide a high fidelity result. However, at this time, convergence has not been met. The appreciable heating demands the utilization of a flexible thermal protection system (TPS) to withstand the heat pulse. Flexible TPS research and development is still very much so in its infancy. New materials and layup structure will need to be investigated in order to protect the payload from the high levels of convective and radiative heating anticipated.

## VI. Conclusions

The analyses presented in this paper give a glimpse into the potential for asymmetric HIADs. The tradeoff between  $\beta$  and  $L/D$  performance is illustrated. When compared to its symmetric counterpart, for a large range of angle of attack, Shifted HIADs present encouraging results with the ability to improve  $L/D$  performance by increasing both lift and drag. For the other asymmetric HIADs analyzed in this study,  $L/D$  was always improved; however it was due to the increase in  $C_L$  only. For the Flat and Biconic OMLs, the change in area was the prevailing asymmetric factor resulting in decreased  $C_D$  values and higher  $\beta$ . However, for nearly all asymmetric HIAD geometries, the trim angle of attack at  $L/D = 0.275$  is lower which has beneficial attributes. Slightly higher  $\beta$  may be considered acceptable in exchange for lower trim angles and/or aerothermodynamic advantages. Furthermore, all asymmetric HIAD configurations were shown to be statically stable during hypersonic flight. Trim lines and  $C_m$  curves justify an array of potential CG locations for each type of configuration. It is also established that both convective and radiative heating will be major factors due to the complex flow experienced. Early estimations indicate that radiative heating may be more significant than convective heating. The aerothermodynamic response for the Shifted HIADs does slightly encourage use over a symmetric counterpart, but the Biconic and Flat HIADs do not. The results do not exhibit the heat transfer benefits that were assumed for these designs which put the results into question. Overall, the aerodynamic performance and or stability benefits intrinsic to asymmetric HIADs may promote their use in future high mass Mars landing missions.

## References

- <sup>1</sup> Braun, R., Manning, R., "Mars Exploration Entry, Descent, and Landing Challenges," *Journal of Spacecraft and Rockets*, Vol. 44, No. 2, March-April 2007, p. 310-323.
- <sup>2</sup> D. W. Way, R. W. Powell, A. Chen, A. D. Stelzner, A. M. San Martin, P. D. Burkhardt, and G. F. Mendeck, "Mars Science Laboratory: Entry, Descent, and Landing System Performance," *IEEE Aerospace Conference*, 2006.
- <sup>3</sup> Adler, M. et al, "Draft Entry, Descent, and Landing Roadmap: Technology Area 09," NASA, November 2010.
- <sup>4</sup> Dwyer-Cianciolo, Alicia M., et al. "Entry, Descent and Landing Systems Analysis Study: Phase 1 Report." (2010).
- <sup>5</sup> Ivanon, M. C., et al, "Entry, Descent, and Landing Systems Analysis Study: Phase 2 Report on Mars Science Laboratory Improvement," NASA/TM-2011-216988, July 2011.
- <sup>6</sup> Steinfeldt, B. A., et al, "High Mass Mars Entry, Descent, and Landing Architecture Assessment," AIAA 2009-6684, AIAA Space 2009 Conference and Exposition, Pasadena, CA, September 2009.
- <sup>7</sup> Drake, B. G. (Editor), "Human Exploration of Mars Design Reference Architecture 5.0," NASA/SP-2009-566, July 2009.
- <sup>8</sup> Andrews, D. G., Cannon, J. H., Lund, E. A., Watry, K. E., "High Mass Mars Entry System: Architecture Design and Technology Development Roadmap," NASA/CR-2009-NNL08AA35C, September 2009.
- <sup>9</sup> Smith, B. P., Tanner, C. L., Mahzari, M., Clark, I. G. Braun, R. D., and Cheatwood, F. M., "A Historical Review of Inflatable Aerodynamic Decelerator Technology Development," IEEEAC 1267, 2010 IEEE Aerospace Conference, Big Sky, MT, March 2010.

- <sup>10</sup> Bloetscher, F., "Aerodynamic Deployable Decelerator Performance-Evaluation Program, Phase II," Goodyear Aerospace Corporation Technical Report, AFFDL TR-67-24, June 1967.
- <sup>11</sup> Rohrschneider, R.R., Braun, R.D., "Survey of Ballute Technology for Aerocapture," *Journal of Spacecraft and Rockets*, Vol. 44, No. 1, January 2007.
- <sup>12</sup> Litton, D. K., Bose, D. M., Cheatwood, F. M., Hughes, S., Wright, H. S., Lindell, M. C., Derry, S.D., and Olds, A., "Inflatable Re-entry Vehicle Experiment (IRVE)-4 Overview," *21st AIAA Aerodynamic Decelerator Systems Technology Conference and Seminar*, Dublin, Ireland, May 2011
- <sup>13</sup> Reed, D.R., *Wingless Flight: The Lifting Body Story*, The University Press of Kentucky, 2002.
- <sup>14</sup> von Karman, T., "Isaac Newton and Aerodynamics," *Journal of the Aeronautical Sciences*, Vol. 9, No. 14, December 1942, pp. 521–522,548.
- <sup>15</sup> Anderson, J. D. J., *Hypersonic and High Temperature Gas Dynamics*, McGraw-Hill, New York, 1989.
- <sup>16</sup> Lees, L., "Hypersonic Flow," Fifth International Aeronautical Conference, Los Angeles, 1955, pp. 247–276
- <sup>17</sup> Christian, J., Manyapu, K., Wells, G., Lafleur, J., Verges, A., and Braun, R., "Sizing of an Engry, Descent, and Landing System for Human Mars Exploration," *AIAA Space 2006 Conference*, San Jose, CA, AIAA Paper 2006-7427, Sept. 2006.
- <sup>18</sup> Cruz, J. R., Cianciolo, A. D., Powell, R. W., Simonsen, L. C., and Tolson, R. H., "Entry, Descent, and Landing Technology Concept Trade Study for Increasing Payload Mass to the Surface of Mars," *Atmospheric Reentry Association*, Mar. 2005.
- <sup>19</sup> Bose D. M., et al., "The Hypersonic Inflatable Aerodynamic Decelerator (HIAD) Mission Applications Study," *AIAA Aerodynamic Decelerator Systems Technology Conference and Seminar*, Daytona Beach, FL, March 2013.
- <sup>20</sup> Bose, D., White, T., Santos, J., Feldman, J., Mahzari, M., Olson, M., and Laub, B., "Initial Assessment of Mars Science Laboratory Heatshield Instrumentation and Flight Data," AIAA Paper 2013-0908, 2013.
- <sup>21</sup> Hollis, B. R. and Borrelli, S., Aerothermodynamics of Blunt Body Entry vehicles. *Progress in Aerospace Sciences*, 48, 42-56, 2012.
- <sup>22</sup> Wright, M. J., Tang, C. Y., Edquist, K. T., Hollis, B. R., Krasa, P., and Campbell, C. A., "A Review of Aerothermal Modeling for Mars Entry Missions," , No. 2010-443, 2010.
- <sup>23</sup> Edquist, K.T., Dyakonov, A.A., Wright, M.J., and Tang, C.Y., "Aerothermodynamic Design of the Mars Science Laboratory Backshell and Parachute Cone," AIAA Paper No. 2009-4078, Jun. 2009.
- <sup>24</sup> Mitcheltree, R.A. and Gnoffo, P.A. "Wake Flow about a MESUR Mars Entry Vehicle," AIAA 94-1958, June 1994.
- <sup>25</sup> Kinney D., "Aerothermal Anchoring of CBAERO Using High Fidelity CFD," AIAA-2007-0608, 45th AIAA Aerospace Sciences Meeting and Exhibit, Reno NV, Jan. 2007.
- <sup>26</sup> Kinney D., "Aero-Thermodynamics for Conceptual Design," AIAA-2004-31, 42nd AIAA Aerospace Sciences Meeting and Exhibit, Reno NV, Jan. 2004.
- <sup>27</sup> M. E. Tauber, "A Review of High-Speed, Convective, Heat-Transfer Computation Methods," NASA TP-2914, 1989.
- <sup>28</sup> M. E. Tauber and K. Sutton, "Stagnation-point Radiative Heating Relations for Earth and Mars Entries," *Journal of Spacecraft and Rockets*, vol. 28, No. 1, 1991, pp. 4042.
- <sup>29</sup> Gnoffo, P. A., Gupta, R. N., and Shinn, J., "Conservation Equations and Physical Models for Hypersonic Air Flows in Thermal and Chemical Nonequilibrium," NASA TP 2867, 1989.
- <sup>30</sup> Gnoffo, P. A., "An Upwind-Biased, Point-Implicit Relaxation Algorithm for Viscous, Compressible Perfect-Gas Flows," NASA TP 2953, 1990
- <sup>31</sup> Mazaheri, A., Gnoffo, P. A., Johnston, C. O., and Kleb, B., "LAURA Users Manual: 5.5-65761," NASA TM, March, 2013.
- <sup>32</sup> Papadopoulos, P., Prahlbu, D., Olynick, D., Chen, Y. K., and Cheatwood, F. M., "CFD Code Validation and Comparisons for Mars Entry Simulations," AIAA Paper 98-0272, AIAA Aerospace Sciences Meeting and Exhibit, Reno, NV, January 1998.
- <sup>33</sup> Queen, E. M., Cheatwood, F. M., Powell, R. W., Braun, R. D., and Edquist, C. T., "Mars Polar Lander Aerothermodynamic and Entry Dispersion Analysis," *Journal of Spacecraft and Rockets*, Vol. 36, No. 3, May-June 1999.
- <sup>34</sup> Gnoffo, P. A., Weilmuenster, K. J., Braun, R. D., and Cruz, C. I., "Influence of Sonic-Line Location on Mars Pathfinder Probe Aerothermodynamics," *Journal of Spacecraft and Rockets*, Vol. 33, No. 2, March-April 1996.
- <sup>35</sup> Roe, P. L., "Approximate Riemann Solvers, Parameter Vectors and Difference Schemes," *Journal of Computational Physics*, Vol. 43, No. 2, 1981.
- <sup>36</sup> Yee, H. C., "On Symmetric and TVD Upwind Schemes," NASA TM-86842, September 1985.
- <sup>37</sup> Pointwise, Inc., "Gridgen Version 15 User Manual", 2012.